Nanoscale

Cite this: *Nanoscale*, 2012, **4**, 6515

www.rsc.org/nanoscale

PAPER

Visible-light-driven photocatalytic carbon-doped porous ZnO nanoarchitectures for solar water-splitting†

Yan-Gu Lin,[ae] Yu-Kuei Hsu,[b] Ying-Chu Chen,[c] Li-Chyong Chen,*[c] San-Yuan Chen[d] and Kuei-Hsien Chen*[ac]

Received 11th July 2012, Accepted 17th August 2012
DOI: 10.1039/c2nr31800h

C-doped ZnO hierarchically porous nanoarchitectures were synthesized *in situ* on indium tin oxide (ITO) through a counter strategy. The PEC performance of the C-doped ZnO nanoarchitectures in the splitting of water without sacrificial reagents was systematically evaluated for the first time. In comparison to other ZnO-based photoanodes in the literature, C-doped ZnO nanoarchitectures exhibit a striking photoresponse. Not only do they have a maximum IPCE value of 95%, but they also have an IPCE at the monochromatic wavelength of 400 nm as high as 26.6%, implying that modification by doping with carbon substantially improves the light utilization and conversion efficiency in the visible region of interest over those obtained using a conventional ZnO structure. This model hybrid photoanode will enable us to design high-activity, high-stability visible-light-driven photoelectrodes in the future.

Introduction

The success of three-dimensionally macroporous nanoarchitectures in the past decade suggests their indispensable role in a wide range of fields, from optical computing and telecommunication to photocatalysts and photovoltaic cells.[1] In particular, increasing the effective optical path length of incident light to promote the effective absorption of solar photons through highly periodic nanoarchitectures may be an effective means of enhancing the efficiency of solar-related applications.[2,3] As a result of the recent ecological and energy crises that are related to our dependence on fossil fuel, interest in the development of novel and nanostructured materials for the production of clean energy is growing.[4,5] Hydrogen is an effective source of energy that can be combined with oxygen in a fuel cell to produce electricity and water without any pollutants. It is therefore an environmentally friendly fuel of the future. However, most hydrogen is produced today by the catalytic reforming of hydrocarbons, which consumes natural resources and generates carbon dioxide as an undesired byproduct.[6,7] The direct conversion of solar energy to hydrogen *via* photoelectrochemical (PEC) water-splitting has the advantages of green processing and energy savings.[8,9] The light-harvesting efficiency of photoelectrodes is of great importance to the generation of hydrogen using solar-powered water-splitting. The evolution of hierarchically porous nanoarchitectures is essential to their huge potential in the efficient solar-driven production of hydrogen because the extraordinary nanostructures of highly specific pore-channel frameworks can significantly improve the confinement and localization of incident light, enhancing the effective interaction of light with photoactive materials.

In the search for a semiconductor that can facilitate the efficient storage of solar energy in the form of hydrogen *via* PEC cells, ZnO remains a favorable material.[10,11] With an appropriate flat band potential, low electrical resistance, nontoxic nature, low cost and resource abundance, the use of ZnO as a photoelectrode in the application of PEC water-splitting at a scale corresponding to the world energy demand is highly desirable.[12] Many studies on ZnO as an oxygen-evolving photoanode for the light-driven decomposition of water have detailed its promising aspects and limitations. As major drawbacks ZnO possesses a quick recombination of photoinduced electron–hole pairs, poor optical absorption ability towards visible-light irradiation and photoinstability in aqueous solution, which intrinsically confine its performance in solar energy conversion.[13] Recently, extensive research efforts have been devoted to overcoming these disadvantages by the surface modification of ZnO, such as the doping of carbon and hybridization with carbon-containing species.[14] Therefore, it is possible that an effective integration of ZnO porous nanoarchitectures and carbon hybridization would lead to a photoanode with enhanced solar-hydrogen efficiency and long-term durability in an aqueous environment. In this article, we aim to combine the above state-of-the-art doping and

[a]*Institute of Atomic and Molecular Sciences, Academia Sinica, Taipei 10617, Taiwan. E-mail: chenkh@pub.iams.sinica.edu.tw*
[b]*Department of Opto-Electronic Engineering, National Dong Hwa University, Hualien, 97401, Taiwan*
[c]*Center for Condensed Matter Sciences, National Taiwan University, Taipei 10617, Taiwan. E-mail: chenlc@ntu.edu.tw*
[d]*Department of Materials Science and Engineering, National Chiao Tung University, Hsinchu 30010, Taiwan*
[e]*Chemical Sciences and Engineering Division, Argonne National Laboratory, IL 60439, USA. E-mail: yglin@anl.gov*
† Electronic supplementary information (ESI) available: Experimental procedure, TEM mapping images, XPS spectrum, UV-vis spectra, and amperometric *I–t* curves of the pure ZnO porous nanoarchitectures. See DOI: 10.1039/c2nr31800h

morphological designing strategies through synthesizing *in situ* hierarchically porous C-doped ZnO. Besides, unlike conventional carbon doping methods, in which C-containing organic molecules serve as the dopant and are added into the ZnO matrix, we adopt a counter strategy for the self-doping of carbon. In our approach Zn precursor is added to polystyrene (PS) opals, which are the source of carbon and facilitate the formation of a porous structure. This soft synthetic strategy allows self-doping and pore-channel formation to be accomplished simultaneously during low-temperature calcination, while the amount and position of the doping elements can be readily controlled under mild conditions. The prepared C-doped ZnO hierarchically porous nanoarchitectures exhibited high absorption capacity and an extended photoinduced electron–hole pair lifetime, rendering a significant photoresponse in the visible region.

The C-doped ZnO hierarchically porous nanoarchitectures were synthesized *in situ* on the ITO substrate by a facile and inexpensive wet-chemical method, using a colloidal crystal templating (CCT) approach (see Fig. S1, ESI†).[1] PS opals were first self-assembled on the ITO substrate and then their voids were infiltrated by Zn precursors; the opal templates were finally removed by calcination at a low-temperature of 300 °C. The microstructural characterization was carried out using several analytical techniques including electron microscopy (EM), X-ray photoelectron spectroscopy (XPS), X-ray absorption spectroscopy (XAS) and UV-vis absorption spectroscopy. The PEC performance of C-doped ZnO hierarchically porous nanoarchitectures in water splitting without sacrificial reagents was also systematically evaluated.

Experimental section

Synthesis

To synthesize C-doped ZnO hierarchically porous nanoarchitectures, 10 wt% PS colloidal suspension (microparticles GmbH, 500 nm) was deposited on the ITO substrate. After evaporation of water from the suspension in an electronic dry-box at room temperature (20–25% RH), PS opals with well-defined structures were formed on the ITO substrate. These PS particle-packed templates were heated at 75–90 °C for 3–6 h to improve the connectivity between the neighboring particles. The zinc precursor solution containing 0.01–0.1 M $Zn(NO_3)_2 \cdot 6H_2O$ (98%, Aldrich) in ethanol was then applied dropwise over the surface of the PS layer several times. These infiltrated samples were then placed in an electronic dry-box (20–25% RH) at room temperature for 4–10 h. Finally, the resulting ZnO/PS composites were heated in air to 300 °C to obtain the C-doped ZnO hierarchically porous nanoarchitectures. Pure ZnO hierarchically porous nanoarchitectures were also prepared by the sol–gel method[15] and then tetrahydrofuron (THF) was used to fully remove the PS before heating (300 °C). For further comparison, conventional ZnO structures (referred to as: random and non-porous ZnO structures) were deposited on the ITO substrate prepared in a manner similar to that described elsewhere.[16]

Characterization

SEM measurements were made on a JEOL 6700 field-emission SEM. XPS spectra were obtained using a Microlab 350 system. For obtaining TEM images, the inverse-opal products on the ITO substrate were scratched and dispersed on a carbon-coated Cu grid and analyzed using a JEOL JEM-2100 TEM system. XAS analyses were performed in beamlines BL17C1 and BL20A1 at the National Synchrotron Radiation Research Center (NSRRC), Taiwan. UV-vis absorption spectra were obtained using a JASCO V-670 instrument. A water-splitting photoelectrode was used as the working electrode with a surface area of 0.5–1 cm^2, a platinum plate was the counter electrode and Ag/AgCl was the reference electrode. All PEC studies were operated in 0.5 M Na_2SO_4 (pH7.0) as a supporting electrolyte medium using an Electrochemical Multichannel Solartron Analytical System. The water-splitting photoelectrode was illuminated with AM 1.5G simulated solar light at 100 mW cm^{-2}.

Results and discussion

Fig. 1 shows the morphology and microstructure of the hierarchical porous nanoarchitectures. The scanning electron microscopy (SEM) image illustrates a continuous oxide framework consisting of an interconnected pore network permeating throughout the structure (see Fig. 1a). The nanoarchitectures fabricated exhibit a uniform pore size of around 360 nm, interconnected by around 220 nm windows between the adjacent pores. These values represent a shrinkage of about 30% during calcination since the PS beads used as sacrificial templates were around 500 nm in size. One of the most significant advantages of the porous nanoarchitectures, which are clearly distinct from the traditional photoelectrodes, is that hierarchical pore-channel networks offer effective contact between incident light and the surface of the photoelectrodes. A high-resolution transmission electron microscopy (HRTEM) image of the ZnO nanoarchitectures is presented in Fig. 1b showing that the spacing between the (101) lattice planes of the hexagonal ZnO crystal is 0.24 nm. Further investigations with elemental mappings *via* energy-filtered TEM reveal uniformly dispersed carbon atoms inside the ZnO porous nanoarchitectures (see Fig. 2a and b). The formation of residual carbon could be attributed to the low calcination temperature of 300 °C, which is not enough for the complete removal of the PS opal template. Besides, TEM elemental mappings with Zn and O have also been supplemented in the ESI (see Fig. S5, ESI†), showing that the Zn and O atoms are homogeneously distributed throughout the structures. To further clarify whether carbon was indeed introduced into the

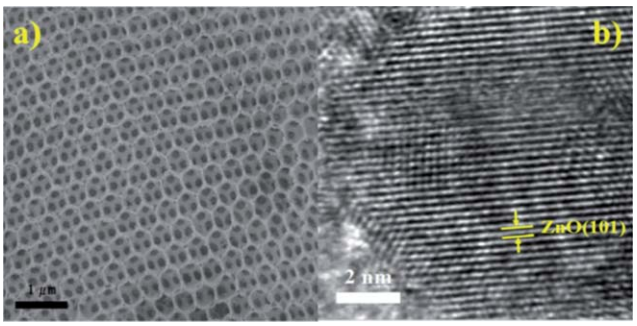

Fig. 1 (a) SEM image and (b) HRTEM image of C-doped ZnO hierarchically porous nanoarchitectures.

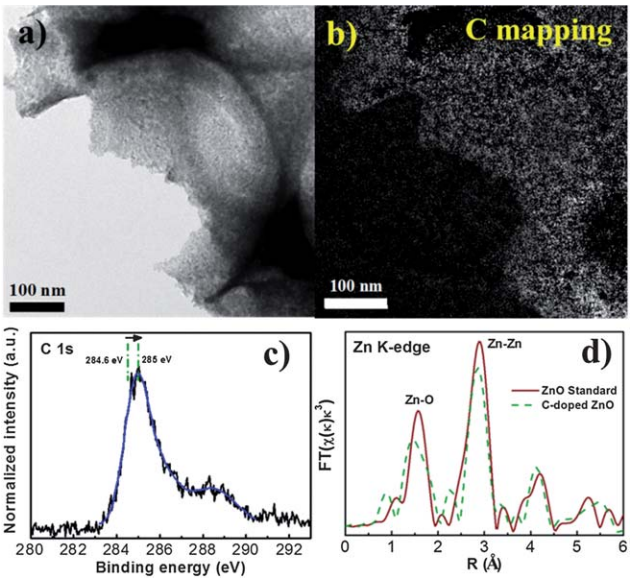

Fig. 2 (a) Typical TEM image of C-doped ZnO hierarchically porous nanoarchitectures. Corresponding energy-filtered TEM (b) carbon mapping image of C-doped ZnO hierarchically porous nanoarchitectures. (c) XPS spectrum of C 1s peak of C-doped ZnO hierarchically porous nanoarchitectures. (d) Zn K-edge EXAFS spectra of C-doped ZnO hierarchically porous nanoarchitectures and pure ZnO standard samples.

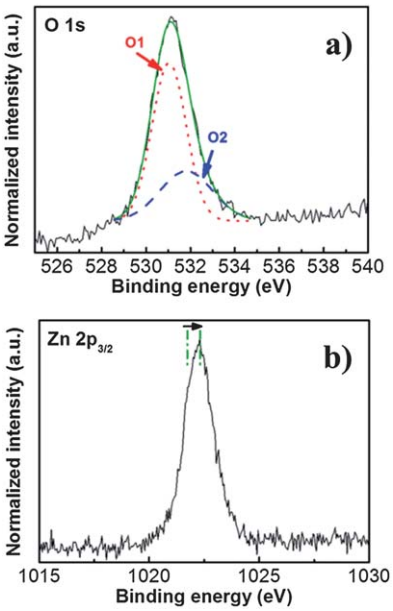

Fig. 3 XPS spectrum of (a) O 1s and (b) Zn 2p3/2 core-level regions for C-doped ZnO hierarchically porous nanoarchitectures. In Fig. 3a, two peaks centered at binding energies of 531.0 and 532.3 eV can be clearly observed. The low binding energy at 531.0 eV, denoted by O1, corresponds to Zn–O bonding, while the higher one of 532.3 eV, denoted by O2, is primarily attributed to the C–O bond. In Fig. 3b, a slight up-shift of the main peak position as compared to pure ZnO (1021.7 eV) is likely to be due to the strong interaction between carbon and ZnO.

lattice, the C-doped ZnO hierarchically porous nanoarchitectures were heated again in air to 600 °C (10 h). XPS measurements were then carried out, the results of which are illustrated in the ESI (see Fig. S6, ESI†).

To gain a better understanding of the electronic structures of the C-doped ZnO hierarchically porous nanoarchitectures, systematic XPS and XAS studies were performed. The C 1s core level spectra of C-doped ZnO hierarchically porous nanoarchitectures in Fig. 2c display a main peak at 285 eV and a shoulder peak around 288.3 eV. The main peak, which is normally located at 284.6 eV, arises from adventitious elemental carbon or graphite-like bonding, while the shoulder peak corresponds to C–O bonding species.[17] Obviously, a slight up-shift of the main peak position with the occurrence of a shoulder peak could be obtained as a result of the strong interaction between carbon and ZnO by means of incorporation of carbon atoms into the ZnO lattice. This indication is further confirmed by the XPS results for O 1s and Zn 2p3/2 (see Fig. 3). Furthermore, it has been reported that if C substitutes for O then the C 1s binding energy shifts to a slightly lower value.[18] However, in the case of C atoms substituted at the Zn site, there is the possibility of the C–O bond with C 1s binding energies higher than for free carbon.[19] It has also been estimated that the energies of C atoms substituted at the O site are prohibitively higher.[19] The absence of any lower energy peak in our XPS spectrum of C 1s core-level regions seems to imply that it is Zn, instead of O, which is substituted by C. The carbon concentration in the C-doped ZnO hierarchically porous nanoarchitectures is estimated to be about 8–10 at% (by XPS measurements).

Extended X-ray absorption fine structure (EXAFS) spectra taken around the Zn K-edge of C-doped ZnO hierarchically porous nanoarchitectures are presented in Fig. 2d. An apparent decrease in the relative intensity and interatomic distance of the first-shell and second-shell (Zn–O and Zn–Zn bonding) over C-doped ZnO hierarchically porous nanoarchitectures could be observed compared to the pure ZnO structure. The reason may mainly be attributed to the strong distortion of the ZnO lattice resulting from the positioning of carbon in the ZnO framework. The slight decrease of the ZnO lattice with C incorporation may suggest that the smaller sized carbon atom has most likely substituted for the larger Zn atom,[20] which is consistent with XPS results. The further fitting results of pure ZnO and carbon-modified ZnO samples at the Zn K-edge have also been carried out (see Table 1). The Debye–Waller factor, σ^2 (more precisely, the mean-square relative displacement), accounts for the thermal and static disorder effects associated with the movement of atoms about their equilibrium (averaged) position. More significant values are observed for carbon-modified ZnO samples at the Zn–O and Zn–Zn coordinations compared to that of pure ZnO samples. The fitting results of the carbon-modified ZnO samples also show a slightly reduced Zn–O bond length and a higher coordination number compared to that of the pure ZnO samples. A possible reason which is likely is the incorporation of carbon atoms into the ZnO lattice. Furthermore, Fig. 4 shows the O K-edge XAS spectra of C-doped ZnO hierarchically porous nanoarchitectures. The spectral features can be interpreted as follows: the region between 530 and 538 eV can be attributed to the hybridization between O 2p and Zn 4s states, followed by the region between 539 and 550 eV, which is due to the hybridization between the O 2p and Zn 4p states.[21] The

Table 1 Results of the fit to Zn K-edge EXAFS data in pure ZnO and carbon-modified ZnO samples[a]

Sample	Shell	N	R_j (Å)	σ^2 (Å^2)	ΔE_0 (eV)	R-factor
ZnO	Zn–O	3.3	1.96	0.003	4.8	0.003
	Zn–Zn	13.2	3.23	0.015	3.9	0.003
Carbon-modified ZnO	Zn–O	3.6	1.94	0.005	1.6	0.005
	Zn–Zn	13.1	3.24	0.016	4.6	0.005

[a] N: coordination number, R_j: bonding distance, σ^2: Debye–Waller factor, ΔE_0: inner potential shift, R: reliability factor for each fitting.

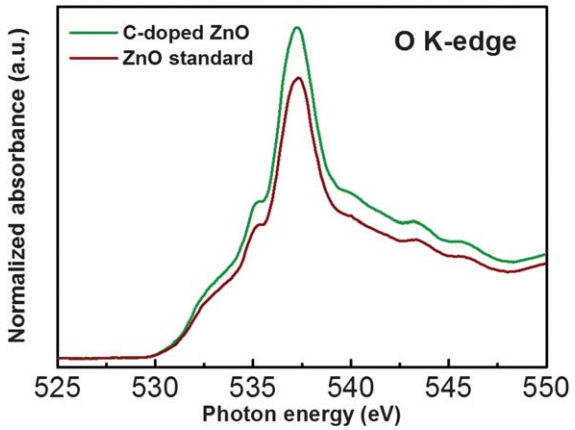

Fig. 4 O K-edge XAS spectra of C-doped ZnO hierarchically porous nanoarchitectures and pure ZnO standard samples.

increase in the relative intensity of the spectral feature at around 531–535 eV observed in C-doped ZnO hierarchically porous nanoarchitectures compared to the pure ZnO structure indicates the increase of the unoccupied density of states (DOS) of O 2p-Zn 4s hybridized states, which may be caused by the strong hybridization of C–O bonds.[21] In addition, the broadening of the absorption peak at ~537 eV over C-doped ZnO hierarchically porous nanoarchitectures in comparison with the pure ZnO structure is assigned to the presence of oxygen vacancies, suggesting that carbon incorporation induces oxygen vacancies in ZnO lattice.[21]

In order to address the quantitative correlation between carbon incorporation and light absorption of the C-doped ZnO hierarchically porous nanoarchitectures we performed incident-photon-to-current-conversion efficiency (IPCE) measurements to study the photo-active wavelength regime as shown in Fig. 5a. In addition to achieve the maximum IPCE value of 95%, it should be noted that the IPCE of C-doped ZnO hierarchically porous nanoarchitectures at the monochromatic wavelength of 400 nm is 26.6% higher than that of traditional ZnO, manifesting that carbon modification substantially improves the light utilization and conversion efficiency in the visible region of interest in comparison with the pure ZnO structure. This result is in good agreement with the UV-vis absorption data. Systematic PEC measurements without sacrificial reagents were carried out to evaluate the characteristics of photoanodes fabricated from C-doped ZnO hierarchically porous nanoarchitectures. Here, a carbon-modified ZnO electrode acts in O_2 evolution as a Pt electrode might act in H_2 evolution. Fig. 5b shows a set of linear sweep voltammagrams without sacrificial reagents in the dark and under light illumination of 100 mW cm^{-2}. Linear sweep voltammagrams in the dark from −0.19 to +1.0 V show the current range of 10^{-7} A cm^{-2}, which is attributed to the double layer current. Under light illumination, the conventional ZnO structures and pure ZnO hierarchically porous nanoarchitectures only yield a photocurrent density of 0.02 and 0.77 mA cm^{-2} at +1.0 V, while the regular C-doped ZnO hierarchically porous nanoarchitectures produce 1 mA cm^2 (see Fig. 5b), which is even superior to that of other ZnO-based or TiO_2-based photoanodes in recent reports.[10,11,22,23] Significantly, it is worth mentioning that the saturated photocurrent can be achieved at a more positive potential in C-doped ZnO hierarchically porous nanoarchitectures, indicating efficient charge separation induced by the microstructural modification of ZnO with carbon under illumination. This can be attributed to the formation of oxygen vacancies resulted from carbon incorporation into the ZnO framework *via* XAS results. The oxygen vacancies may work as electron acceptors and trap the photogenerated electrons temporarily to reduce the surface recombination of electrons and holes. Here, the oxygen vacancies can be considered to be the trap centers to prolong the lifetime of electron–hole pairs in the ZnO photoanode. Furthermore, in order to quantitatively

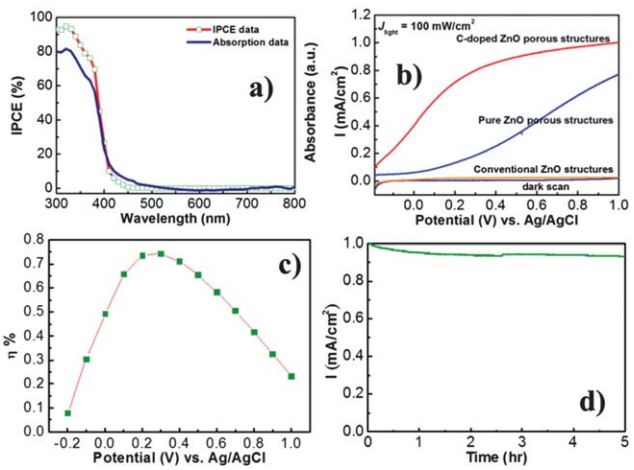

Fig. 5 (a) Measured IPCE and UV-vis absorption spectra of C-doped ZnO hierarchically porous nanoarchitectures in the region of 300 to 800 nm. (b) Linear sweep voltammagrams, collected at a scan rate of 10 mV s^{-1} at applied potentials from −0.19 to +1.0 V (*vs.* Ag/AgCl) for C-doped ZnO hierarchically porous nanoarchitectures in the dark, conventional ZnO structures, pure ZnO hierarchically porous nanoarchitectures and C-doped ZnO hierarchically porous nanoarchitectures at 100 mW cm^{-2}. (c) Photoconversion efficiency of the PEC cell with carbon-modified ZnO inverse opal photoelectrode as a function of applied potential. (d) Amperometric *I–t* curves of the C-doped ZnO hierarchically porous nanoarchitectures collected at a potential of +1.0 V (*vs.* Ag/AgCl) for 5 h.

explore the photoactivity of C-doped ZnO hierarchically porous nanoarchitectures, the efficiency (η) of photon-to-hydrogen generation is calculated using an equation in which the contribution due to the applied potential is subtracted from the total efficiency.[11] The plot of efficiency *versus* applied potential (see Fig. 5c) shows the maximum value of efficiency is 0.75% at an applied potential of +0.3 V, which is higher than the recently reported values for ZnO-based or TiO_2-based photoanodes.[10,11,22] Last but not least, the advantage of C-doped ZnO hierarchically porous nanoarchitectures is further exemplified by the good stability in the photo-oxidation process at pH = 7 (see Fig. 5d), which is significantly superior to the 15% reduction after 1 h only of continuous running for pure ZnO hierarchically porous nanoarchitectures (see Fig. S7, ESI†). Since the photogenerated holes are the dominating carrier for ZnO materials during the photocorrosion reaction, in our system, the holes rapidly transferring to the solution for water–oxidation reaction may successfully facilitate the reduction of the photocorrosion due to the high efficiency of charge separation induced by the microstructural modification of ZnO with carbon. Therefore, the merit of the cooperative effect, *i.e.* optical amplification and surface hybridization, can be unambiguously highlighted here *via* IPCE, linear sweep voltammagrams, photon-to-hydrogen conversion efficiency and stability data.

In this work, a doping mechanism that may be useful in forming C-doped ZnO porous nanoarchitectures is suggested. PS is assumed to play an important role in the formation of these doped porous structures. First, the infiltration with Zn precursors within the voids of PS opals leads to the adsorption and nucleation of primary amorphous Zn^{2+} on the surface of the PS particles. In other words, the PS particles serve as nucleation seeds for the final ZnO particles *via* thermal calcinations. Through calcination in air, ZnO crystallization, the combustion of carbon and the rearrangement of atoms (Zn, O and C) which occurred, the substitution of a fraction of the Zn atoms in the ZnO lattice with carbon atoms was resulted. The polycrystalline C-doped ZnO porous nanoarchitectures were, therefore, synthesized. All of the above inferences suggested that the carbon doping in ZnO can be achieved by a rapid combustion process during the procedure for the removal of PS and carbon doping is an effective way to improve the photocatalytic activity in the visible light region. However, the real doping mechanism may be more complicated and more research needs to be done to elucidate it. The investigation on this issue is in progress.

Conclusions

An easy route for the *in situ* preparation of C-doped ZnO hierarchically porous nanoarchitectures on the ITO as photoanodes was successfully demonstrated. Hierarchical porous nanoarchitectures demonstrate the idea of increasing the optical path length of solar light through pore-channel networks, a wide range of carbon modifications can enhance the separation of photoinduced electron–hole pairs, the absorption of visible-light and the photostability of a ZnO photoanode. This model hybrid photoanode structure will be useful in the development of high-activity, high-stability, visible-light-driven photoelectrodes.

Acknowledgements

This work was supported by the National Science Council, Ministry of Education, Academia Sinica (Core Facilities), Taiwan, and AOARD under AFOSR, US. We gratefully thank NSC, IAMS, NTU, and National Synchrotron Radiation Research Center for financial support for this project.

Notes and references

1 A. Stein, F. Li and N. R. Denny, *Chem. Mater.*, 2008, **20**, 649.
2 S. Nishimura, N. Abrams, B. A. Lewis, L. I. Halaoui, T. E. Mallouk, K. D. Benkstein, J. van de Lagemaat and A. J. Frank, *J. Am. Chem. Soc.*, 2003, **125**, 6306.
3 J. I. L. Chen, G. von Freymann, S. Y. Choi, V. Kitaev and G. A. Ozin, *Adv. Mater.*, 2006, **18**, 1915.
4 T. Ishida and M. Haruta, *Angew. Chem., Int. Ed.*, 2007, **46**, 7154.
5 K. Sivula, R. Zboril, F. Le Formal, R. Robert, A. Weidenkaff, J. Tucek, J. Frydrych and M. Gratzel, *J. Am. Chem. Soc.*, 2010, **132**, 7436.
6 D. R. Palo, R. A. Dagle and J. D. Holladay, *Chem. Rev.*, 2007, **107**, 3992.
7 Y. G. Lin, Y. K. Hsu, S. Y. Chen, Y. K. Lin, L. C. Chen and K. H. Chen, *Angew. Chem., Int. Ed.*, 2009, **48**, 7586.
8 K. Honda and A. Fujishima, *Nature*, 1972, **238**, 37.
9 N. S. Lewis, *Nature*, 2001, **414**, 589.
10 X. Yang, A. Wolcott, G. Waang, A. Sobo, R. C. Fitzmorris, F. Qian, J. Z. Zhang and Y. Li, *Nano Lett.*, 2009, **9**, 2331.
11 Y. G. Lin, Y. K. Hsu, Y. C. Chen, S. B. Wang, J. T. Miller, L. C. Chen and K. H. Chen, *Energy Environ. Sci.*, 2012, DOI: 10.1039/c2ee22185c.
12 E. Hendry, M. Koeberg, B. O'Regan and M. Bonn, *Nano Lett.*, 2006, **6**, 755.
13 M. A. Fox and M. T. Dulay, *Chem. Rev.*, 1993, **93**, 341.
14 S. Cho, J. W. Jang, J. S. Lee and K. H. Lee, *CrystEngComm*, 2010, **12**, 3929.
15 R. V. Nair and R. Vijaya, *J. Phys. D: Appl. Phys.*, 2007, **40**, 990.
16 K. Keis, E. Magnusson, H. Lindstrom, S. E. Lindquist and A. Hagfeldt, *Sol. Energy Mater. Sol. Cells*, 2002, **73**, 51.
17 Y. G. Lin, Y. K. Hsu, C. T. Wu, S. Y. Chen, K. H. Chen and L. C. Chen, *Diamond Relat. Mater.*, 2009, **18**, 433.
18 H. Pan, J. B. Yi, L. Shen, R. Q. Wu, J. H. Yang, J. Y. Lin, Y. P. Feng, J. Ding, L. H. Van and J. H. Yin, *Phys. Rev. Lett.*, 2007, **99**, 127201.
19 S. T. Tan, X. W. Suna, Z. G. Yu, P. Wu, G. Q. Lo and D. L. Kwong, *Appl. Phys. Lett.*, 2007, **91**, 072101.
20 S. Akbar, S. K. Hasanain, M. Abbas, S. Ozcan, B. Ali and S. Ismat Shah, *Solid State Commun.*, 2011, **151**, 17.
21 S. Krishnamurthy, C. McGuinness, L. S. Dorneles, M. Venkatesan, J. M. D. Coey, J. G. Lunney, C. H. Patterson, K. E. Smith, T. Learmonth, P. A. Glans, T. Schmitt and J. H. Guo, *J. Appl. Phys.*, 2006, **99**, 08M111.
22 A. Wolcott, W. A. Smith, T. R. Kuykendall, Y. Zhao and J. Z. Zhang, *Small*, 2009, **5**, 104.
23 Y. J. Hwang, A. Boukai and P. D. Yang, *Nano Lett.*, 2009, **9**, 410.